coatings

MDPI

Article

The Microstructure of Zr/Nb Nanoscale Multilayer Coatings Irradiated with Helium Ions

Roman Laptev [1,*], Ekaterina Stepanova [1], Natalia Pushilina [1], Egor Kashkarov [1], Dmitriy Krotkevich [1], Anton Lomygin [1], Alexey Sidorin [2], Oleg Orlov [2] and Vladimir Uglov [3]

[1] Division for Experimental Physics, National Research Tomsk Polytechnic University, 634050 Tomsk, Russia
[2] Dzhelepov Laboratory of Nuclear Problems, Joint Institute for Nuclear Research, 141980 Dubna, Russia
[3] Department of Solid State Physics, Belarusian State University, 220006 Minsk, Belarus
* Correspondence: laptevrs@tpu.ru; Tel.: +7-913-852-3733

Abstract: The effect of helium ion irradiation on the microstructure and properties of composites based on Zr/Nb nanoscale multilayer coatings (NMCs) was studied. X-ray diffraction (XRD), transmission electron microscopy (TEM), and variable-energy Doppler broadening spectroscopy (DBS) were used for the in-depth analysis of defects in the irradiated NMCs. After irradiation of the Zr/Nb NMCs with helium ions at a 10^{17} ion/cm^2 dose, the layered structure was generally retained, but the internal stresses in the layers were increased, which caused wave-like distortion in the ion deposition zone. The Zr/Nb NMCs with an individual layer thickness of 25 nm were characterized by the smallest microstress changes, but single blisters were formed in the near-surface region. The microstructure of the Zr/Nb NMCs with a layer thickness of 100 nm exhibited relatively smaller changes upon helium ion irradiation. The prevailing positron-trapping center was the reduced-electron-density area at the interfaces before and after irradiation of the Zr/Nb NMCs regardless of the layer thickness. However, the layer thickness affected the DBS parameter profiles depending on the positron energy, which was probably due to the different localization of implanted ions within the layers or at the interfaces.

Keywords: nanoscale multilayer coatings; helium ion irradiation; microstructure; positron annihilation; radiation defects; nanohardness

Citation: Laptev, R.; Stepanova, E.; Pushilina, N.; Kashkarov, E.; Krotkevich, D.; Lomygin, A.; Sidorin, A.; Orlov, O.; Uglov, V. The Microstructure of Zr/Nb Nanoscale Multilayer Coatings Irradiated with Helium Ions. *Coatings* **2023**, *13*, 193. https://doi.org/10.3390/coatings13010193

Academic Editor: Engang Fu

Received: 16 December 2022
Revised: 11 January 2023
Accepted: 13 January 2023
Published: 15 January 2023

1. Introduction

The development of functional-graded materials (FGMs) is one of the prospective areas in the construction of radiation- and hydrogen-tolerant materials with advanced properties [1–4]. A high radiation tolerance of FGMs can be achieved by producing different specific dimension defects for sink creation and increasing diffusion mobility. Radiation-induced defects and associated variations in the physical and mechanical properties of FGMs have been actively studied over the past decade [5–7]. Multilayer functionally graded coatings with different crystalline structures are considered as potential materials with high radiation resistance, since vacancy-type defects and interstitial atoms can recombine at the interfaces [8–12]. Based on this, alternating metallic multilayers with different crystal structures (BCC, FCC, and HCP) can be used for creating radiation-tolerant nanoscale multilayer coatings (NMCs) [13–15]. Therefore, NMCs are also promising structural materials for advanced nuclear reactors and aerospace applications [16–18]. The formation of defects in NMCs is significantly lower than in single-layer films under identical ion irradiation conditions [19–23]. NMCs have shown a high resistance to helium ion irradiation [24,25], and helium bubbles are almost never observed in these systems after irradiation [26,27]. Moreover, a higher content of incoherent interfaces decreases the formation of helium bubbles in NMCs [23,28]. Nanoscale multilayer coatings based on Zr/Nb exhibit a high radiation tolerance under proton and helium ion irradiation as well as under the imitation of neutron exposure by heavy ion irradiation [1,5,6,13–15,29–31], which is crucial for fusion

reactor construction materials. However, the essence and mechanism of this phenomenon has not yet been thoroughly studied. The evolution of the microstructure and mechanical properties of Zr/Nb NMCs under irradiation requires further investigation, especially with the application of positron annihilation techniques, which will provide complementary information on the defect structure of NMCs depending to the individual layer thickness and irradiation conditions [32–34]. Thus, the aim of the work was an experimental study of the effect of helium ion irradiation on the microstructure, defect state, and mechanical properties of Zr/Nb NMCs with different individual layer thicknesses.

2. Materials and Methods

NMCs with alternating layers of Zr and Nb were fabricated by magnetron sputtering in a special facility at the Weinberg Research Center of the National Research Tomsk University of Technology (TPU, Tomsk, Russia). A (111)-oriented single-crystal silicon substrate was fixed in the experimental chamber using an axial rotation system. The residual pressure in the chamber was 2×10^{-3} Pa. The layers were deposited in an Ar atmosphere with a working pressure of 0.3 Pa. Before deposition, the substrate was cleaned with Ar ions for 30 min at a voltage of 2.5 kV and an ion current of 2.5 mA. A series of Zr/Nb NMC samples with individual layer thicknesses of 25 nm (Zr/Nb NMCs 25/25) and 100 nm (Zr/Nb NMCs 100/100) were prepared. The total coating thickness for all samples was 1.1 ± 0.2 μm.

The NMCs were irradiated in a DC-60 heavy ion accelerator (Institute of Nuclear Physics, Kazakhstan, Almaty) with a quasi-perpendicular helium ion beam with an energy of 40 keV and a fluence of 2×10^{17} cm^{-2}. An analysis of the impact of the implanted ions on the defect structures in the functionally graded nano-sized Zr/Nb metal multilayer systems was performed using the software package SRIM-2013 [35]. Simulations were carried out for the Zr/Nb multilayer systems with different individual layer thicknesses for the radiation conditions specified above. The total number of particles was $1.5 \cdot 10^5$. The threshold displacement energies were 40 eV for the Zr and 78 eV for the Nb layers [36]. According to SRIM simulations, using these parameters of helium ion irradiation, Bragg peaks in the range of 150 ± 60 nm could be obtained.

The layer-by-layer analysis of structural defects was performed by Doppler broadening spectroscopy (DBS) using a variable-energy positron beam at the JINR, DLNP in Dubna, Russia. The beam was 5 mm in diameter and had an intensity of 10^6 e^+/sec. An energy range from 0.1 to 25 keV was used for the implanted positrons. From the monoenergetic positron implantation profile in a quasi-infinite solid, as described by the Makhovian profile [37], the average positron implantation depth was determined. The annihilation of γ radiation was detected by a GEM25P4-70 (AMETEK ORTEC, Oak Ridge, TN, USA) high-purity germanium detector with an energy resolution of 1.20 keV for the 511 keV line. The obtained DBS spectra were analyzed using the SP-11 software, which calculated the S and W parameters. The S parameter describes the annihilation of low-momentum electron–positron pairs that occurs mainly in vacancy-type defects and is determined as the ratio of the central area of the annihilation line to the total peak area. The W parameter allows the identification of the chemical environment of the annihilation site and is defined by the ratio of the area under the wings of the annihilation peak to its total area.

An Ion Slicer EM-09100IS (JEOL, Akishima, Japan) was used for thin foil preparation at an 8 kV acceleration voltage and a 1.5–4 etching angle. The microstructural investigation of the thin foils was performed with a JEM-2100F electron microscope (JEOL, Akishima, Japan). The phase composition was determined by XRD using an XRD-7000S (Shimadzu, Japan) in Bragg–Brentano geometry from 20 to 75° with a scanning rate of 5.0 deg/min [38]. A Table Top Nanoindentation System (CSM Instruments, Peseux, Switzerland) was applied to determine the nanohardness and Young's modulus at a load of 5 mN and an exposure time of 30 s. The average of at least 20 indentations was calculated and presented.

3. Results

The concentration of helium ions and the displacement per atom (dpa) distribution calculated according to SRIM are shown in Figure 1. The ion distribution plot for the Zr/Nb NMCs 25/25 (Figure 1a) showed that the maximum concentration of implanted helium ions (~20 at.%) was at 190 ± 80 nm. Due to the different threshold displacement energies, the damage distribution plot has a sawtooth shape with a peak damage value of 6 dpa in the second and third zirconium layers at a depth of 95 and 140 nm. The maximum damage for the niobium layers was 3 dpa. For the Zr/Nb NMCs 100/100 (Figure 1b), the implantation depth was 160 ± 60 nm (~20 at.%) (first Zr layer). The damage distribution plot for the Zr/Nb NMCs 100/100 demonstrated a maximum value of ~6 dpa in the first Zr layer at a 115 nm depth.

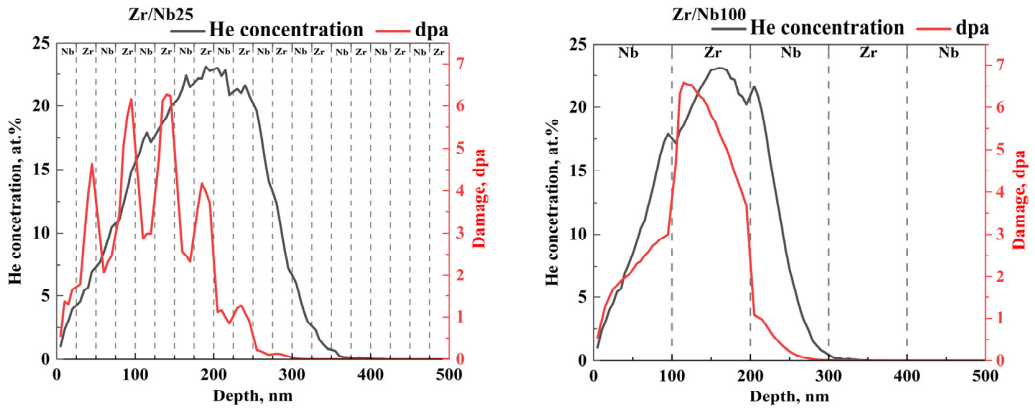

(**a**) (**b**)

Figure 1. Helium ion and damage distribution in Zr/Nb NMCs 25/25 (**a**) and Zr/Nb NMCs 100/100 (**b**) as calculated by SRIM-2013 code.

A layer-by-layer DBS analysis of the Zr/Nb NMCs with layer thicknesses of 25 and 100 nm before and after irradiation was performed by evaluating the S and W parameters as a function of the positron energy (Figure 2).

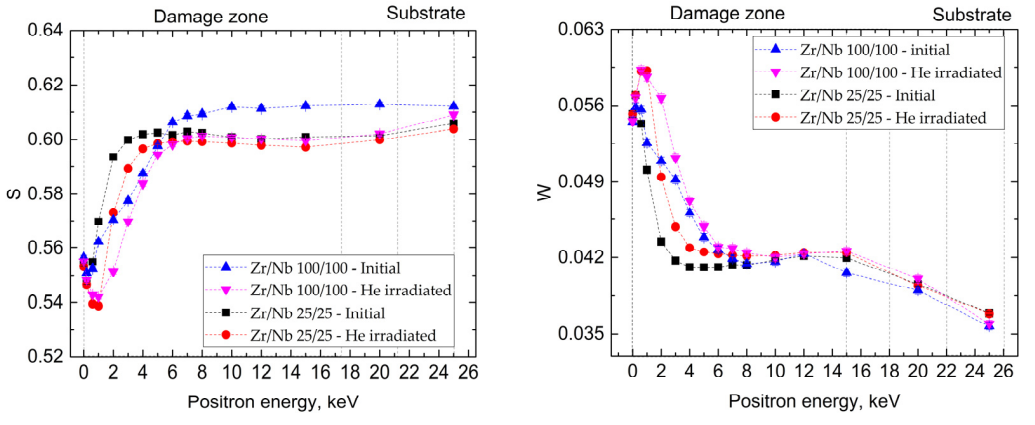

(**a**) (**b**)

Figure 2. Dependence of the S (**a**) and W (**b**) parameters on the positron energy for Zr/Nb NMCs before and after helium ion irradiation.

Significant differences in the S(E) and W(E) curves were observed for the different individual layer thicknesses of the NMCs Zr/Nb. The Zr/Nb NMCs 25/25 were characterized by a sharp transition between positron annihilation in the first niobium layer (0.1 to 1 keV) and positron annihilation in the vicinity of zirconium [13]. Due to the higher positron affinity of zirconium, as well as the presence of a reduced electron

density at the Zr/Nb interface, the positrons were predominantly annihilated in the zirconium vicinity near the interface [14]. At positron energies less than 3 keV, the positrons were annihilated in the vicinity of niobium for the Zr/Nb NMCs 100/100. A further increase in the positron energy led to a slight rise in the S parameter, while the W parameter decreased. In this case, the S parameter changed insignificantly in the range from 7 to 26 keV, while the W parameter showed a decreasing tendency from 12 to 26 keV.

Since both the S and W parameters depend on type and amount of the positron-trapping center, an S = f(W) plot was used to determine the cause of these changes [39]. The prevailing positron-trapping center will be similar if the experimental values of the S and W parameters for the dataset are in a straight line. In the S = f(W) plot, a change in the slope of the straight line indicates a change in the prevailing positron-trapping center.

The analysis of the S = f(W) dependence showed that the probability of positron annihilation in the silicon substrate increased when the positron energy exceeded 20 keV (Figure 3). It was also observed that in the 7–26 keV region, the W parameter was similar for both the Zr/Nb NMCs 25/25 and Zr/Nb NMCs 100/100. Meanwhile, the S parameters significantly differed. The S parameter for the Zr/Nb NMCs 25/25 in the range from 6 to 20 keV was essentially higher than that of the Zr/Nb NMCs 100/100, which was probably due to the growth of the volume fraction of the reduced electron density caused by increasing the number of interfaces. This was confirmed by the S = f(W) analysis, since the experimental values in the 7–26 keV region for both systems were in the same area.

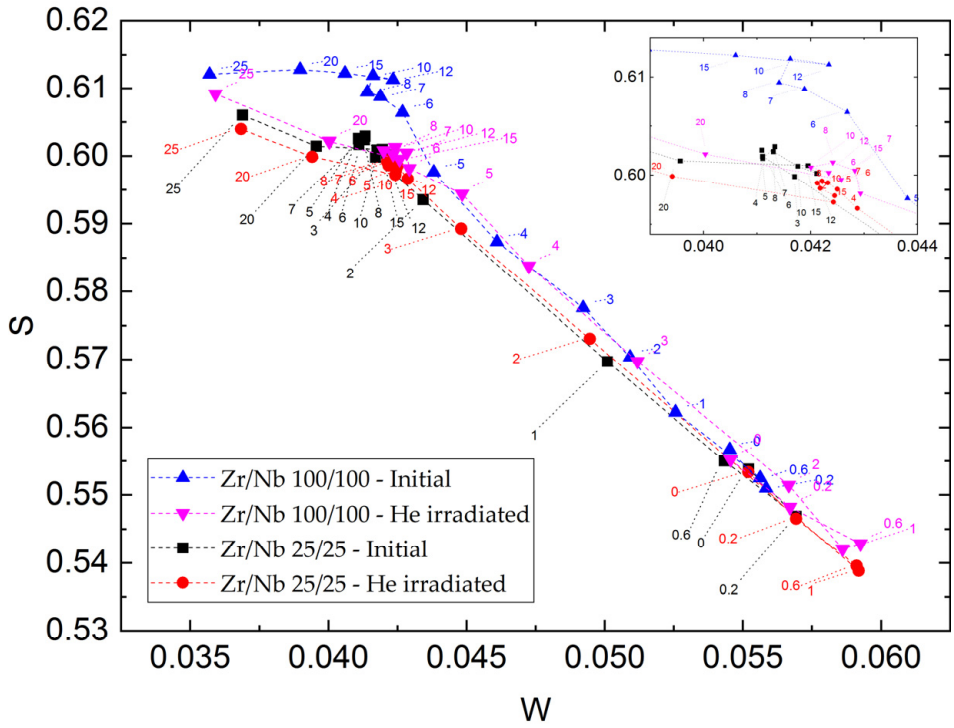

Figure 3. The S = f(W) plot for Zr/Nb NMCs at different positron energies before and after helium ion irradiation.

The helium ion irradiation of Zr/Nb NMCs 25/25 did not lead to a significant rise in the S parameter in the whole range of positron energies with respect to the unirradiated material (Figures 2 and 3). For the minimum positron energies up to 0.2 keV, the values of the S and W parameters before and after irradiation were practically unchanged. A maximum decrease in the S parameter for more than 5.5 % was observed at a positron energy of 1 keV. In the range from 1 to 5 keV, the S parameter value fluently increased up to the unirradiated level, and it further changed insignificantly. Variations in the W parameter in relation to the S parameter had opposite trends, which caused the

experimental S = f(W) values for the Zr/Nb NMCs 25/25 before and after helium ion irradiation to not essentially differ.

The Zr/Nb NMCs 100/100 after irradiation were characterized by more significant changes in the S(E) and W(E) dependences. Major differences were observed in the region of (0.6–4) keV (S↓W↑), which was slightly less than the expected zone of ion deposition (5–7 keV e+). In the range from 5 to 25 keV, the W parameter values before and after irradiation of the Zr/Nb NMCs 100/100 were almost the same, but the S parameter was almost 2% lower than the values before irradiation, and this was similar to the Zr/Nb NMCs 25/25.

The DBS parameter profiles' dependencies on the positron energy were substantially different, which was probably due to the particularities of the ion localization in the layer bulk and in the interface vicinity. The analysis of the S = f(W) dependence showed the preservation of one prevailing type of positron-trapping center after irradiation with helium ions in the Zr/Nb NMCs regardless of the thickness. For the Zr/Nb NMCs with individual layer thicknesses of 100 nm, the probability of positron annihilation in the bulk of the layers and at the interfaces varied significantly after irradiation.

The microstructure of the initial as-deposited samples of both studied series was described in detail in [13,14]. It was shown that structures with alternating layers of zirconium and niobium were obtained. The formed layers were characterized by clear distinguishable boundaries between the individual layers of Zr and Nb and the absence of visible defects. The thicknesses of the alternating layers were (25 $\pm$ 5) and (100 $\pm$ 20) nm for the Zr/Nb 25/25 and Zr/Nb 100/100, respectively. A more detailed study of the transverse sections of the as-deposited Zr/Nb NMCs demonstrated that in the bulk of each Zr and Nb layer, nanoscale columnar grains with a size of (10–50) nm comparable with the layer thickness were observed. The average grain sizes varied from 20 to 50 nm for the Zr/Nb NMC 100/100 samples and from 10 to 25 nm for the samples of the Zr/Nb NMCs 25/25. Incoherent interfaces between Zr and Nb layers were revealed by high-resolution TEM studies.

The microstructures of the Zr/Nb 25/25 and Zr/Nb 100/100 NMCs after irradiation with helium ions with a dose of 2×10^{17} ions/cm^2 are shown in Figure 4. It can be seen that after irradiation with helium ions, all the NMCs studied were characterized by the presence of reflections from different planes of the α-Zr phase and the β-Nb phase. In addition, as a result of irradiation, there was a significant increase in the internal stresses for all the studied Zr/Nb NMCs, which was confirmed by the selected area electron diffraction (SAED) pattern (Figure 4a,b). At the same time, for a smaller thickness of individual layers (Zr/Nb 25/25 samples), the value of the internal stresses in the near-surface regions was higher. This led to wave-like distortions of the near-surface layers. In this case, for the Zr/Nb 25/25 samples, the formation of single blisters was observed. At the same time, irradiation of the Zr/Nb NMCs 100/100 with helium ions led to less-pronounced changes.

The high-resolution TEM studies showed that for all the Zr/Nb NMCs after irradiation with helium ions, the interfaces remained incoherent, there were significant internal stresses in the layers, and the presence of amorphous regions was also characteristic for the samples (Figure 4e,f). A specific feature of the regions where the maximum effect of the helium ions occurred was the presence of helium bubbles. Previously, such bubbles were observed in [40].

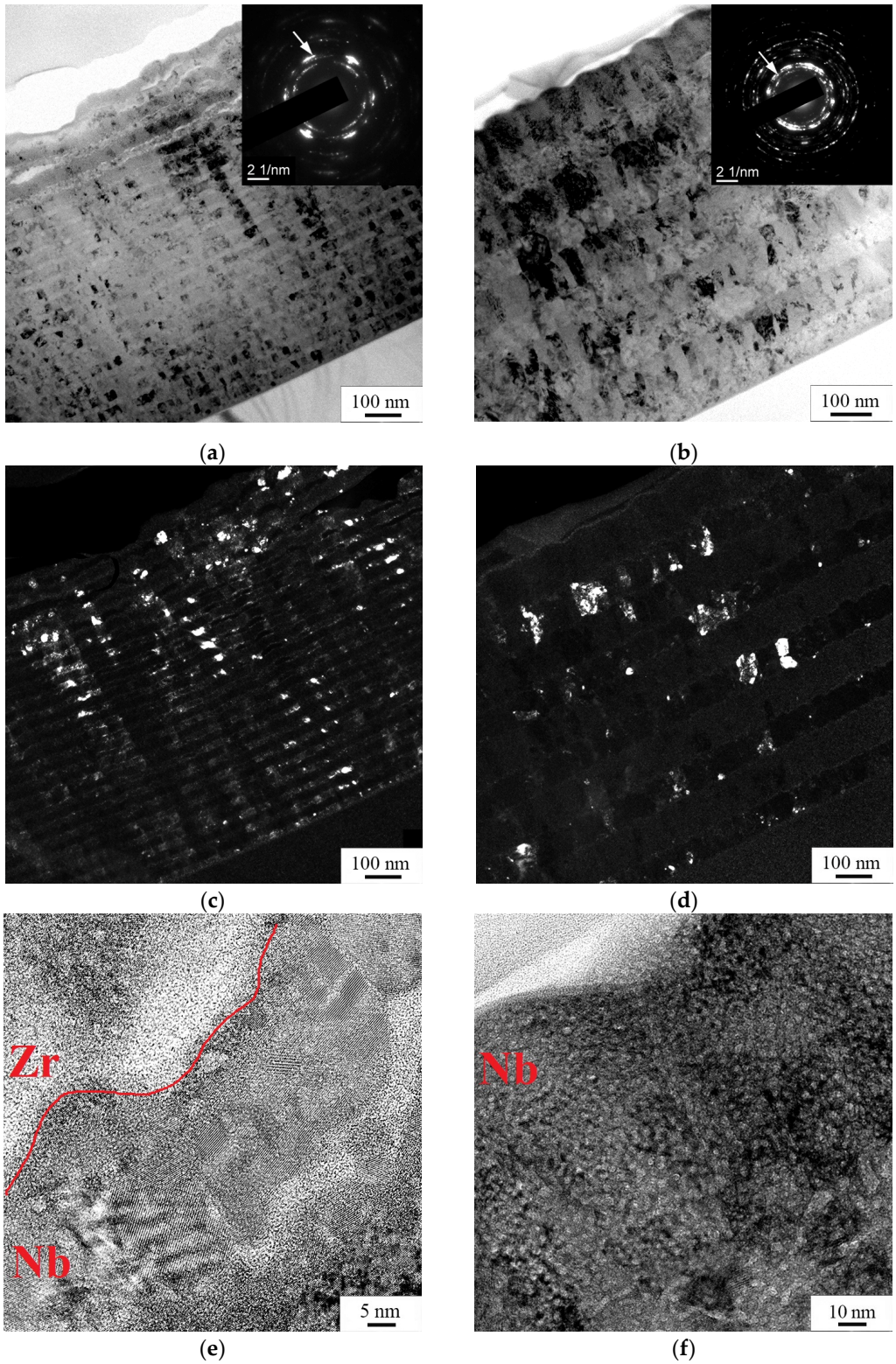

Figure 4. Cross-sectional microstructure of the Zr/Nb 25/25 (**a**,**c**,**e**) and Zr/Nb 100/100 (**b**,**d**,**f**) NMCs after irradiation with helium ions with a dose of 2×10^{17} ions/cm^2: bright-field images and corresponding SAED (**a**,**b**), dark-field image in (220) Nb_β reflection (indicated by arrow in (**a**)) (**c**), dark-field image in (110) Zr_α reflection (indicated by arrow in (**b**)) (**d**), dark-field image in (110) Zr_α reflection (indicated by arrow) (**d**), HR TEM images (**e**,**f**).

The X-ray diffraction analysis showed that the Zr/Nb NMCs with individual layer thicknesses of 25 and 100 nm demonstrated a strong Zr(002) and Nb(110) texture (Figure 5). It was found that there were residual stresses of a different nature in the initial coating samples, which affected the interplanar spacing (d-spacing) of the observed Zr(002) and Nb(110) diffraction peaks. Figure 5 shows the positions (blue dash-dotted lines) of the reference Zr(002) and Nb(110) diffraction peaks related to the unstressed material (data taken from the PDF4+ 2021 database; PDF cards: Zr #8-1477, Nb #34-0370) with corresponding d-spacings of 2.585 and 2.336 Å. The initial Zr/Nb coatings were characterized by a shift in the Zr (002) diffraction peak towards higher angles, corresponding to the presence of tensile lateral stresses, whereas the Nb (110) peak was characterized by a shift towards lower angles, corresponding to the presence of compressive lateral stresses. The appearance of residual stresses was associated with the different crystal structures (hcp and bcc) of Zr and Nb and a mismatch between the lattice parameters. In general, the residual stresses increased with decreasing the thickness of the individual layers due to the higher density of interfaces [31]. Obviously, the response of the Zr/Nb NMCs to helium ion irradiation depended on the interaction between the observed residual stresses and the radiation-induced distortions (defect formation) that were also observed by TEM.

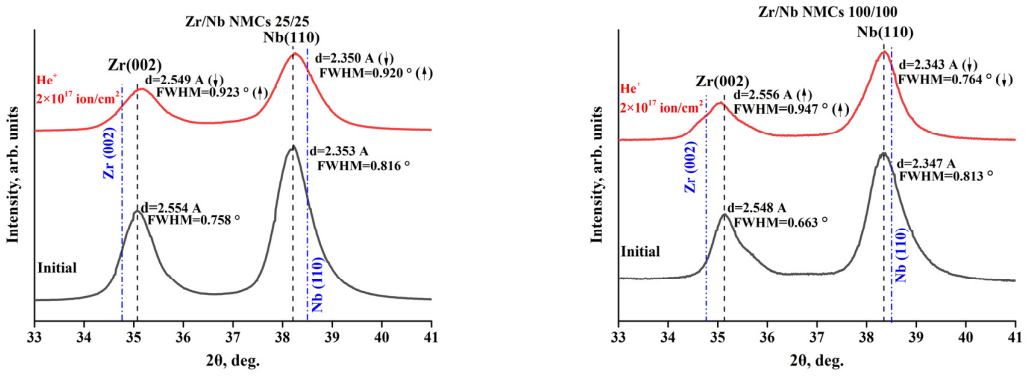

(**a**) (**b**)

Figure 5. Dependence of the S (**a**) and W (**b**) parameter on the positron energy for Zr/Nb NMCs before and after helium ion irradiation.

Irradiation with helium ions at a dose of 2×10^{17} ions/cm^2 led to a change in the residual stresses for the Zr layers depending on the individual layer thickness. For the Zr(002) 25 nm sample, a decrease in the d-spacing from 2.554 Å to 2.549 Å was observed (Figure 5a), corresponding to the increase in the tensile lateral stresses, whereas for the Zr(002) 100 nm sample, the same dose led to an increase in the d-spacing from 2.548 Å to 2.553 Å (Figure 5b), which was caused by the relaxation of the residual lateral stresses. The irradiated Nb layers showed a decrease in the d-spacing regardless of the thickness of the individual layers, which was attributed to the relaxation of the residual lateral stresses. Additionally, a change in the diffraction patterns associated with the broadening of the diffraction peaks was observed. The full width at half maxima (FWHM) value can be affected by the microstrain and the size of coherently diffracting domains attributed to the formation of radiation-induced defects as vacancy and interstitial clusters, dislocation loops, amorphization zones, etc. [41]. An increase in the FWHM was observed for the diffraction reflections of the Zr(002) 25 nm, Nb(110) 25 nm, and Zr(002) 100 nm samples. However, a decrease in the FWHM was observed for the Nb(110) 100 nm reflection (Figure 5b), indicating a decrease in the microstresses and/or an increase in the size of the coherently diffracting domains in the Nb layers. From the X-ray diffraction analysis, it can be seen that the Zr layers showed a more pronounced response to irradiation with helium ions, which was associated with a redistribution of the residual stresses and an increase in the FWHM value, both for the thickness of an individual layer of 25 nm and 100 nm.

The nanohardness was found to decrease after irradiation with helium ions in the Zr/Nb NMCs 25/25. For the Zr/Nb NMCs 100/100, there was practically no change in the nanohardness, and the results were within the acceptable error. Thus, for the Zr/Nb NMCs 100/100, the nanohardness before irradiation was 600 ± 40 HV; after irradiation, it became equal to 530 ± 30 HV. For the Zr/Nb NMCs 25/25, the nanohardness value changed as a result of irradiation from 980 ± 45 HV to 730 ± 30 HV. Irradiation with helium ions led to an increase in the elastic modulus (E) of the Zr/Nb NMCs 100/100 by 40% compared to the corresponding non-irradiated specimens. At the same time, for the Zr/Nb NMC 25/25 samples, the change in the elastic modulus was insignificant: before irradiation E = 160 ± 20 GPa, and after irradiation E = 173 ± 20 GPa.

The change in the nanohardness of the Zr/Nb system after irradiation with helium ions could have been caused by a number of reasons, including the formation of voids, the presence of amorphous regions (which can act as dislocation sinks), the formation of helium bubbles, helium interstitial insertions, and the evolution of the microstructure of the interface between the layers. In the case of the Zr/Nb NMCs 25/25, the decrease in the nanohardness was due to the partial degradation of the multilayer system caused by blister formation as a result of irradiation. The nanohardness results were well in agreement with the current understanding that the evolution of the hardness and microstructure of multilayer materials after irradiation strongly depends on the layer thickness and interface structure [40,42].

The helium ion irradiation with a dose of 10^{17} ion/cm^2 had a specific effect on the microstructure and mechanical characteristics of the composites based on nanoscale multilayer Zr/Nb systems. Although after irradiation there was no mixing of the multilayers, and the interfaces remained incoherent, there was a significant increase in the internal stresses and the presence of amorphous regions. It was shown that the presence of high internal stresses led to wave distortions in the layers in the near-surface region. In addition, this area contained helium bubbles. The shifts of the main XRD reflections after helium ion irradiation revealed a change in the interplanar distance in the Zr and Nb layers with the appearance of mechanical stresses with different signs. These changes were more pronounced for the Zr/Nb NMCs with a thickness of individual layers of 25 nm. This system was characterized by single-blister formation in the near-surface regions and the smallest changes in the XRD diffraction pattern after irradiation. The thickness of the individual layers affected the change in the mechanical properties of the Zr/Nb NMCs. Irradiation increased the elastic modulus while having almost no impact on the nanohardness for the systems with a layer thickness of 100 nm, whereas the opposite happened for the systems with a layer thickness of 25 nm. The irradiation of the Zr/Nb NMCs with helium ions did not lead to significant increase in the S parameter nor a decrease in the W parameter regardless of the individual layer thickness above unirradiated levels. In this case, the depth distribution profiles of these parameters were significantly different, which was probably due to the peculiarities of the localization of implanted ions in the layer bulk and in the vicinity of interfaces. The prevailing positron-trapping center was maintained after helium ion irradiation in the Zr/Nb NMCs, regardless of the thickness. Additional first-principle calculations (DFT) and positron annihilation lifetime spectrometry (PALS) with positron beams are required for the detailed identification of positron-trapping centers. The data obtained confirmed the enhanced radiation tolerance of the multilayer nanoscale systems, since the interfaces acted as effective sinks for radiation-induced defects.

4. Conclusions

The microstructure and mechanical characteristics of helium-ion-irradiated composites based on nanoscale multilayer Zr/Nb coatings were studied. The following conclusions were obtained:

1. The Zr/Nb NMCs demonstrated a high radiation tolerance under helium ion irradiation up to 10^{17} ion/cm^2. After irradiation, the interfaces remained incoherent, and amorphization took place in some regions. No significant difference in the irradiation

resistance was found for the Zr/Nb coatings with individual layer thicknesses of 25 and 100 nm.

2. The irradiation with helium ions resulted in lattice distortions of the hcp Zr and bcc Nb phases, leading to the generation of internal stresses. The latter caused a wave-like morphology of the near-surface layer and corresponding helium bubble formation.

3. Generally, the nanohardness decreased while the elastic modulus increased after irradiation of the Zr/Nb NMCs.

Thin layers had a greater sink efficiency due to them having the highest number of interfaces, but the microstructure of the thick layers was more stable under irradiation up to 10^{17} ion/cm^2. The studied nanoscale multilayer Zr/Nb systems had an enhanced radiation tolerance, making them promising as structural materials for the aerospace, hydrogen, and nuclear industries.

Author Contributions: R.L. conducted the organization of the experimental procedure and preparation of the manuscript. E.S. carried out the microstructure analysis using TEM. N.P. performed and analyzed the results of the mechanical tests. A.L. examined the samples using the GD-OES method. D.K. and E.K. provided the SRIM calculations and the XRD analysis. A.S. and O.O. performed the layer-by-layer analysis using positron spectroscopy methods. V.U. carried out the helium irradiation and a comprehensive analysis of the received data and prepared the manuscript for publication. All authors have read and agreed to the published version of the manuscript.

Funding: This work was funded by the Russian Science Foundation, research project No. 20-79-10343.

Institutional Review Board Statement: Not applicable.

Informed Consent Statement: Not applicable.

Data Availability Statement: Not applicable.

Acknowledgments: The TEM and STEM research was carried out using the equipment of the CSU NMNT TPU, supported by the RF MES project No. 075-15-2021-710.

Conflicts of Interest: The authors declare no conflict of interest.

References

1. Daghbouj, N.; Sen, H.S.; Callisti, M.; Vronka, M.; Karlik, M.; Duchon, J.; Čech, J.; Havránek, V.; Polcar, T. Revealing Nanoscale Strain Mechanisms in Ion-Irradiated Multilayers. *Acta Mater.* **2022**, *229*, 117807. [CrossRef]
2. Mishin, I.P.; Grabovetskaya, G.P.; Stepanova, E.N.; Laptev, R.S.; Teresov, A.D. Hydrogen Effect on the Defect Structure Formation in the Zr-wt.% Nb Alloy Under Pulsed Electron Beam Irradiation. *Russ. Phys. J.* **2019**, *62*, 854–860. [CrossRef]
3. Stepanova, E.N.; Grabovetskaya, G.P.; Mishin, I.P.; Bulinko, D.Y. Structure and Mechanical Properties of a Zr-1Nb Alloy, Obtained by the Method of Severe Plastic Deformation. Mater. *Today Proc.* **2015**, *2*, 365–369.
4. Li, H.; Ma, D.; Wang, H.; Yun, D.; Hao, Z.; Deng, J.; Zhang, R.; Li, Z. Microstructure and Oxidation Behavior of CrCN/TiSiCN Nano-Multilayer Coatings on Zircaloy in High-Temperature Steam. *Corros. Sci.* **2023**, *211*, 110883. [CrossRef]
5. Callisti, M.; Lozano-Perez, S.; Polcar, T. Structural and Mechanical Properties of γ-Irradiated Zr/Nb Multilayer Nanocomposites. *Mater. Lett.* **2016**, *163*, 138–141. [CrossRef]
6. Callisti, M.; Karlik, M.; Polcar, T. Competing Mechanisms on the Strength of Ion-Irradiated Zr/Nb Nanoscale Multilayers: Interface Strength versus Radiation Hardening. *Scr. Mater.* **2018**, *152*, 31–35. [CrossRef]
7. Zinkle, S.J.; Snead, L.L. Designing Radiation Resistance in Materials for Fusion Energy. *Annu. Rev. Mater. Res* **2014**, *44*, 241–267. [CrossRef]
8. Ham, B.; Zhang, X. High Strength Mg/Nb Nanolayer Composites. *Mater. Sci. Eng. A* **2011**, *528*, 2028–2033. [CrossRef]
9. Yang, G.H.; Zhao, B.; Gao, Y.; Pan, F. Investigation of Nanoindentation on Co/Mo Multilayers by the Continuous Stiffness Measurement Technique. *Surf. Coat. Technol.* **2005**, *191*, 127–133. [CrossRef]
10. Lu, Y.Y.; Kotoka, R.; Ligda, J.P.; Cao, B.B.; Yarmolenko, S.N.; Schuster, B.E.; Wei, Q. The Microstructure and Mechanical Behavior of Mg/Ti Multilayers as a Function of Individual Layer Thickness. *Acta Mater.* **2014**, *63*, 216–231. [CrossRef]
11. Zhang, J.Y.; Lei, S.; Liu, Y.; Niu, J.J.; Chen, Y.; Liu, G.; Zhang, X.; Sun, J. Length Scale-Dependent Deformation Behavior of Nanolayered Cu/Zr Micropillars. *Acta Mater.* **2012**, *60*, 1610–1622. [CrossRef]
12. Lomygin, A.D.; Laptev, R.S.; Krotkevich, D.G. Positron Annihilation Analysis of Nanosized Metal Coatings Zr/Nb after He+ Ion Irradiation. In Proceedings of the 8th International Congress on Energy Fluxes and Radiation Effects, Tomsk, Russia, 2–8 October 2022; pp. 1203–1207. [CrossRef]

13. Laptev, R.; Stepanova, E.; Pushilina, N.; Svyatkin, L.; Krotkevich, D.; Lomygin, A.; Ognev, S.; Siemek, K.; Doroshkevich, A.; Uglov, V. Distribution of Hydrogen and Defects in the Zr/Nb Nanoscale Multilayer Coatings after Proton Irradiation. *Materials* **2022**, *15*, 3332. [CrossRef]
14. Laptev, R.; Svyatkin, L.; Krotkevich, D.; Stepanova, E.; Pushilina, N.; Lomygin, A.; Ognev, S.; Siemek, K.; Uglov, V. First-Principles Calculations and Experimental Study of H+-Irradiated Zr/Nb Nanoscale Multilayer System. *Metals* **2021**, *11*, 627. [CrossRef]
15. Laptev, R.; Lomygin, A.; Krotkevich, D.; Syrtanov, M.; Kashkarov, E.; Bordulev, Y.; Siemek, K.; Kobets, A. Effect of Proton Irradiation on the Defect Evolution of Zr/Nb Nanoscale Multilayers. *Metals* **2020**, *10*, 535. [CrossRef]
16. Zhang, X.; Hattar, K.; Chen, Y.; Shao, L.; Li, J.; Sun, C.; Yu, K.; Li, N.; Taheri, M.L.; Wang, H.; et al. Radiation Damage in Nanostructured Materials. *Prog. Mater. Sci.* **2018**, *96*, 217–321. [CrossRef]
17. Beyerlein, I.J.; Caro, A.; Demkowicz, M.J.; Mara, N.A.; Misra, A.; Uberuaga, B.P. Radiation Damage Tolerant Nanomaterials. *Mater. Today* **2013**, *16*, 443–449. [CrossRef]
18. Yang, L.X.; Zheng, S.J.; Zhou, Y.T.; Zhang, J.; Wang, Y.Q.; Jiang, C.B.; Mara, N.A.; Beyerlein, I.J.; Ma, X.L. Effects of He Radiation on Cavity Distribution and Hardness of Bulk Nanolayered Cu-Nb Composites. *J. Nucl. Mater.* **2017**, *487*, 311–316. [CrossRef]
19. Yu, K.Y.; Liu, Y.; Fu, E.G.; Wang, Y.Q.; Myers, M.T.; Wang, H.; Shao, L.; Zhang, X. Comparisons of Radiation Damage in He Ion and Proton Irradiated Immiscible Ag/Ni Nanolayers. *J. Nucl. Mater.* **2013**, *440*, 310–318. [CrossRef]
20. Chen, F.; Tang, X.; Huang, H.; Liu, J.; Li, H.; Qiu, Y.; Chen, D. Surface Damage and Mechanical Properties Degradation of Cr/W Multilayer Films Irradiated by Xe^{20+}. *Appl. Surf. Sci.* **2015**, *357*, 1225–1230. [CrossRef]
21. Demkowicz, M.J.; Hoagland, R.G.; Hirth, J.P. Interface Structure and Radiation Damage Resistance in Cu-Nb Multilayer Nanocomposites. *Phys. Rev. Lett.* **2008**, *100*, 136102. [CrossRef]
22. Misra, A.; Demkowicz, M.J.; Zhang, X.; Hoagland, R.G. The Radiation Damage Tolerance of Ultra-High Strength Nanolayered Composites. *Jom* **2007**, *59*, 62–65. [CrossRef]
23. Fu, E.G.; Carter, J.; Swadener, G.; Misra, A.; Shao, L.; Wang, H.; Zhang, X. Size Dependent Enhancement of Helium Ion Irradiation Tolerance in Sputtered Cu/V Nanolaminates. *J. Nucl. Mater.* **2009**, *385*, 629–632. [CrossRef]
24. Demkowicz, M.J.; Wang, Y.Q.; Hoagland, R.G.; Anderoglu, O. Mechanisms of He Escape during Implantation in CuNb Multilayer Composites. *Nucl. Instrum. Methods Phys. Res. Sect. B Beam Interact. Mater. Atoms* **2007**, *261*, 524–528. [CrossRef]
25. Fu, E.G.; Li, N.; Misra, A.; Hoagland, R.G.; Wang, H.; Zhang, X. Mechanical Properties of Sputtered Cu/V and Al/Nb Multilayer Films. *Mater. Sci. Eng. A* **2008**, *493*, 283–287. [CrossRef]
26. Demkowicz, M.J.; Bhattacharyya, D.; Usov, I.; Wang, Y.Q.; Nastasi, M.; Misra, A. The Effect of Excess Atomic Volume on He Bubble Formation at Fcc–Bcc Interfaces. *Appl. Phys. Lett.* **2010**, *97*, 161903. [CrossRef]
27. Li, N.; Mara, N.A.; Wang, Y.Q.; Nastasi, M.; Misra, A. Compressive Flow Behavior of Cu Thin Films and Cu/Nb Multilayers Containing Nanometer-Scale Helium Bubbles. *Scr. Mater.* **2011**, *64*, 974–977. [CrossRef]
28. Fu, E.G.; Misra, A.; Wang, H.; Shao, L.; Zhang, X. Interface Enabled Defects Reduction in Helium Ion Irradiated Cu/V Nanolayers. *J. Nucl. Mater.* **2010**, *407*, 178–188. [CrossRef]
29. Sen, H.S.; Polcar, T. Vacancy-Interface-Helium Interaction in Zr-Nb Multi-Layer System: A First-Principles Study. *J. Nucl. Mater.* **2019**, *518*, 11–20. [CrossRef]
30. Sen, H.S.; Polcar, T. Helium Migration in Zr-Nb Multilayers under Electric Field. *J. Nucl. Mater.* **2021**, *555*, 153133. [CrossRef]
31. Daghbouj, N.; Sen, H.S.; Č'ižek, J.; Lorinč'ik, J.; Karl'ik, M.; Callisti, M.; Čech, J.; Havránek, V.; Li, B.; Krsjak, V.; et al. Characterizing Heavy Ions-Irradiated Zr/Nb: Structure and Mechanical Properties. *Mater. Des.* **2022**, *219*, 110732. [CrossRef]
32. Bordulev, I.; Kudiiarov, V.; Svyatkin, L.; Syrtanov, M.; Stepanova, E.; Č'ižek, J.; Vlček, M.; Li, K.; Laptev, R.; Lider, A. Positron Annihilation Spectroscopy Study of Defects in Hydrogen Loaded Zr-1Nb Alloy. *J. Alloys Compd.* **2019**, *798*, 685–694. [CrossRef]
33. Slugen, V.; Degmova, J.; Sojak, S.; Petriska, M.; Noga, P.; Krsjak, V. On the Limitations of Positron Annihilation Spectroscopy in the Investigation of Ion-Implanted FeCr Samples. *Metals* **2021**, *11*, 1689. [CrossRef]
34. Krsjak, V.; Degmova, J.; Sojak, S.; Slugen, V. Effects of Displacement Damage and Helium Production Rates on the Nucleation and Growth of Helium Bubbles–Positron Annihilation Spectroscopy Aspects. *J. Nucl. Mater.* **2018**, *499*, 38–46. [CrossRef]
35. Ziegler, J.F.; Ziegler, M.D.; Biersack, J.P. SRIM–The Stopping and Range of Ions in Matter. *Nucl. Instrum. Methods Phys. Res. Sect. B Beam Interact. Mater. Atoms* **2010**, *268*, 1818–1823. [CrossRef]
36. Konobeyev, A.Y.; Fischer, U.; Korovin, Y.A.; Simakov, S.P. Evaluation of Effective Threshold Displacement Energies and Other Data Required for the Calculation of Advanced Atomic Displacement Cross-Sections. *Nucl. Energy Technol.* **2017**, *3*, 169–175. [CrossRef]
37. Vehanen, A.; Saarinen, K.; Hautojärvi, P.; Huomo, H. Profiling Multilayer Structures with Monoenergetic Positrons. *Phys. Rev. B* **1987**, *35*, 4606. [CrossRef]
38. Syrtanov, M.; Garanin, G.; Kashkarov, E.; Pushilina, N.; Kudiiarov, V.; Murashkina, T. Laboratory X-ray Diffraction Complex for in Situ Investigations of Structural Phase Evolution of Materials under Gaseous Atmosphere. *Metals* **2020**, *10*, 447. [CrossRef]
39. Kuznetsov, P.V.; Mironov, Y.P.; Tolmachev, A.I.; Bordulev, Y.S.; Laptev, R.S.; Lider, A.M.; Korznikov, A.V. Positron Spectroscopy of Defects in Submicrocrystalline Nickel after Low-Temperature Annealing. *Phys. Solid State* **2015**, *57*, 219–228. [CrossRef]

40. Liang, X.Q.; Wang, Y.Q.; Zhao, J.T.; Wu, S.H.; Feng, X.B.; Wu, K.; Zhang, J.Y.; Liu, G.; Sun, J. Size-Dependent Microstructure Evolution and Hardness of He Irradiated Nb/Zr Multilayers under Different Ion Doses. *Mater. Sci. Eng. A* **2019**, *764*, 138259. [CrossRef]
41. Ungar, T. Microstructural Parameters from X-Ray Diffraction Peak Broadening. *Scr. Mater.* **2004**, *51*, 777–781. [CrossRef]
42. An, B.; Wang, Y.; Wu, K.; Zhang, J.; Liu, G.; Sun, J. Interface-Controlled Mechanical Properties and Irradiation Hardening in Nanostructured Cr75Al25/Zr Multilayers. *Mater. Sci. Eng. A* **2022**, *850*, 143558. [CrossRef]